Asian Journal of Chemistry; Vol. 24, No. 3 (2012), 1069-1074

ASIAN JOURNAL OF CHEMISTRY

www.asianjournalofchemistry.co.in

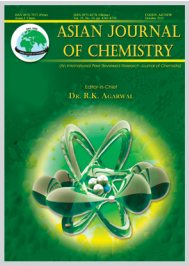

Preparation and Characterization of Multi-Component Catalysts for the Oxidative Coupling of Methane

KAI HUANG*, SONGBO NI and KEQIANG LU

School of Chemistry and Chemical Engineering, Southeast University, Nanjing 211189, P.R. China

*Corresponding author: Tel: +86 25 83795839; E-mail: huangk@seu.edu.cn

(*Received*: 4 February 2011; *Accepted*: 7 November 2011) AJC-10596

A multi-component catalyst Na-Mn-Zr-W-S-P/SiO_2 is prepared and tested in a fixed-bed microreactor without inert gases as thinners. The average methane conversion and the C_2 hydrocarbon selectivity in the oxidative coupling of methane are about 35 and 70 %, respectively. The yield of C_2 hydrocarbon is more than 25 %. The catalysts are characterized by X-ray diffraction, X-ray photoelectron spectroscopy, Fourier transform infrared spectroscopy and scanning electron microscopy. Mn_2O_3 is suggested to be the main active species in the catalysts, while the addition of Zr further activates the methane molecules. The addition of W and P efficiently improves C_2 selectivity and inhibits deep-oxidation of SiO_2. Sodium easily combines with WO_4.

Key Words: Preparation, Characterization, Oxidative coupling of methane, Multi-component catalysts.

INTRODUCTION

The oxidative coupling of methane (OCM), one of the direct catalytic methods for the conversion of abundant natural gases to higher-value chemicals and fuels, especially ethylene, continues to attract considerable research interest. Since ethylene was first produced by Keller[1] through the oxidative coupling of methane, efforts had been made world-wide to screen, understand the mechanism and improve the catalysts for the reaction.

In studies carried out thus far, many kinds of potential oxidative coupling of methane catalysts have been applied[2-4], including alkaline-earth metal oxides, lanthanide oxides, transition metal oxides, *etc*. Research has generally been directed towards searching for new and efficient catalysts, especially multi-component ones, which mix different components and improve the reaction performance. Manganese, tungsten and sodium, which have been proven to be promising modifiers in oxidative coupling of methane catalysts, are widely used as the main elements for these components. The catalyst $Mn/Na_2WO_4/SiO_2$[5-7] has been reported to be a particularly effective one, allowing about 20 % methane conversion and 80 % C_{2+} selectivity in the oxidative coupling of methane process. The material is obtained in single-pass mode and is stable for up to 97 h. Another catalyst, Mn/Na_2SO_4-SiO_2, was studied by Wang *et al.*[8]. For this material, the following with optimum reaction conditions were found: T = 1138 K, CH_4/O_2 = 3 (mol ratio), GHSV = 9600 mL g^{-1} h^{-1}. Such a catalyst yields about 32.7 % CH_4 conversion and 20 % C_{2+} yield. Aside from manganese, tungsten and sodium are widely used as the main catalyst components; zirconium-based catalysts have also attracted much attention[9,10]. Similar to the oxides of titanium, manganese and bismuth, sodium chloride-promoted ZrO_2 exhibits noticeable C_{2+} selectivity[11] and it has been suggested that promoted ZrO_2 catalysts, as well as other chlorine-containing ones, could exhibit high performance if the precursors of the active components underwent drastic physical and chemical changes during the preparation process.

Based on previous research[12-14], the main objective of this paper is to prepare silica-supported multi-component catalysts consisting of Na, Mn, Zr, W, S and P. The performance of the catalysts is measured and the roles of the various chemical components in relation to their influence in the oxidative coupling of methane are studied.

EXPERIMENTAL

Catalyst preparation: The multi-component catalysts were prepared by an incipient wetness impregnation method. An aqueous solution with appropriate concentrations of Na_2CO_3, Na_2SO_4, $Na_4P_2O_7$ and Na_2WO_4 was added to silica gel and then dried at 423 K for 3 h, followed by calcination in air at 823 K for 2 h and 1173 K for 6 h. The catalyst was crushed and impregnated with $ZrOCl_2$ and $Mn(CH_3COO)_2$ by the wetness impregnation method, after which it was evaporated to dryness. The catalyst was dried in air at 423 K for 2 h and calcined at 823 K for 2 h and 1173 K for 6h. The samples were finally crushed and sieved through a 20-40 mesh.

Reactor system: The catalytic performance test was performed in a two-stage quartz fixed-bed microreactor with an upper segment size of $\phi 7 \times 1.5$ mm, length of 250 mm and a lower segment size of $\phi 3 \times 1$ mm, length of 250 mm. A two-stage quartz fix-bed microreactor can more effectively minimize the occurence of product side reactions compared to a one-stage fix-bed one. The catalyst powder (0.3 g, 20-40 mesh) was placed in the quartz liner and retained by quartz wool above and below the catalyst bed. The remaining space in the reactor below the catalyst was filled with quartz wool to reduce the free volume and minimize product side reactions.

The reaction conditions were set as follows: the temperature was 1023-1123 K, CH_4/O_2 (mol ratio) was 3 and the GHSV was about 30000-35000 mL g^{-1} h^{-1}. The reaction products were analyzed using two on-line 102G gas chromatographs and the carrier gas was argon. Both a 5A molecular sieve (60-80 mesh) and a 402 organic support (60-80 mesh) were used for the stationary phases and a thermal conductivity detector was used as the detector.

Characterization: The X-ray diffraction (XRD) patterns of the fresh and used multi-component catalysts were obtained with a Rigaku Geigerflex D/MAX-B diffractometer system using CuK_α monochromatic radiation. The unit was operated at 40 KV and 50 mA. Qualitative analysis of the chart was undertaken by contrasting the results with the on-line computer standard chart database.

X-Ray photoelectron spectroscopy (XPS) was used to determine the elements on the surface of catalysts, their valences and their states. Samples were tested with a VG ESCALAB MK II X-ray photoelectron spectroscope. The XP spectra were acquired with $AlK_\alpha 1$, 2 (1486.6 eV) radiation. The resolution was higher than 0.1 eV.

The Fourier transform infrared (FT-IR) spectra of the catalysts were recorded by a Bruker IFS 85 FTIR spectrometer with a mid-infrared spectral range. Each sample was mixed with potassium bromide prior to the analysis.

Scanning electron microscopy (SEM) studies of the catalysts were carried out using a JSM-T20 (Japan) scanning electron microscope. The catalyst samples were homogeneously dispersed in solvent and then coated with gold in a vacuum evaporator prior to the analysis.

RESULTS AND DISCUSSION

The different formulations of the 25 multi-component catalysts were prepared by means of an orthogonal design and five of them were selected for testing and characterization. Table-1 shows the composition of the five multi-component catalysts and their reactivity behaviours.

X-Ray diffraction: The XRD patterns of the multi-component catalysts are shown in Fig. 1. The α-cristobalite phase is shown by the peaks present at the 2θ values of 21.8, 36.0 and 31.3, while the peaks of the tridymite phase are present at 2θ values of 21.6, 20.5 and 23.3. Both the α-cristobalite and tridymite phases can be found in the a, c, d and e patterns, while only the tridymite phase is observed in the b pattern. Patterns a and e show more tridymite than α-cristobalite, whereas, in patterns c and d, the opposite is true. The amorphous phase presented in the silica support changes to the α-cristobalite phase after the addition of Na_2SO_4 and Na_2WO_4 and calcination at high temperatures. Sop-16 performs worse than the four other catalysts (Table-1) and no α-cristobalite phase can be observed in it because of its lower Na_2SO_4 and Na_2WO_4 contents. The results illustrate that the α-cristobalite phase is the active carrier of the multi-component catalysts. Aside from the α-cristobalite and tridymite phases, significant amounts of the crystalline phases of Mn_2O_3, Na_2SO_4, Na_2WO_4 and $Na_2Zr(PO_4)_2$ are present in the catalysts. The presence of the Na_2WO_4 crystalline phase shows that Na has a higher affinity to WO_4. Mn is converted into Mn_2O_3, similar to findings by Ji *et al.*[15]. Zirconium and P are presented mainly in the form of $Na_2Zr(PO_4)_2$; this was reported in a previous study[10]. Sulfur exists as Na_2SO_4 on the surface of the catalysts. Some quartz is also observed on Fop-18 and Fop-27, the presence of which is associated with temperature jumps when the catalysts were calcined. The quartz has no effect on the reaction performance of the catalysts. In Table-2, the crystalline phases of the different multi-component catalysts are presented (the contents decrease from left to right). Characteristic peaks of crystalline phases are given in Table-3.

TABLE-1
SAMPLING CATALYSTS

Catalyst	Molecular content, 10^3 mol/g SiO_2						X_{CH_4} (%)	S_{C2} (%)	Y_{C2} (%)
	Na	S	W	P	Zr	Mn			
Xop-15	1.8921	0.7283	0.0545	0.1324	0.0000	0.6120	35.99	74.40	26.78
Sop-16	6.1204	0.0529	0.0805	0.9604	0.3370	0.2705	6.21	73.03	4.54
Fop-18	2.7380	0.9620	0.2470	0.0868	1.1243	0.3742	36.54	73.07	26.70
Fop-21	3.5397	1.7537	0.0000	0.0161	0.6808	0.4944	37.79	73.50	27.78
Fop-27	5.6543	0.2900	0.1450	0.4653	0.8103	0.6112	35.22	71.72	25.26

Reaction conditions: catalyst loading = 0.3 g, flow rate = 40 cm^3 min^{-1}, CH_4 = 25 %, O_2 = 75 %, reaction temperature = 1069 K.

TABLE-2
CRYSTALLINE PHASES IN DIFFERENT MULTI-COMPONENT OCM CATALYSTS

Catalyst	Crystalline phases
Xop-15	α-Cristobalite, tridymite, Na_2SO_4, Mn_2O_3, Na_2WO_4
Sop-16	Tridymite, Na_2WO_4, Na_2SO_4
Fop-18	α-Cristobalite, tridymite, Na_2SO_4, Mn_2O_3, Na_2WO_4, $Na_2Zr(PO_4)_2$, quartz
Fop-21	α-Cristobalite, Na_2SO_4, tridymite, Mn_2O_3, $Na_2Zr(PO_4)_2$
Fop-27	α-Cristobalite, tridymite, quartz, Na_2WO_4, Na_2SO_4, Mn_2O_3, $Na_2Zr(PO_4)_2$

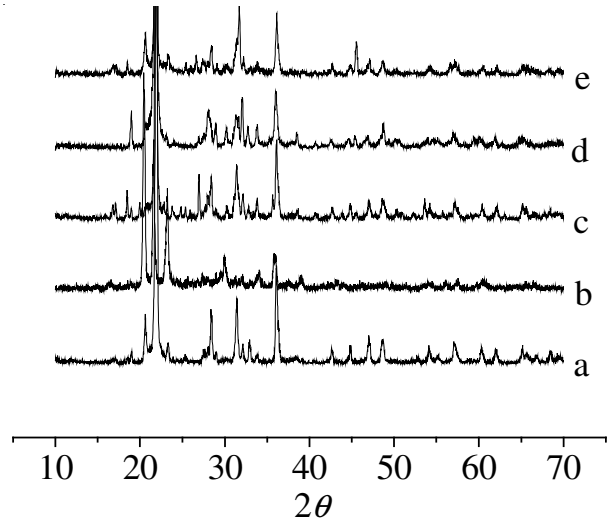

Fig. 1. XRD patterns of different catalysts (a) Xop-15, (b) Sop-16 (c) Fop-18 (d) Fop-21 (e) Fop-27

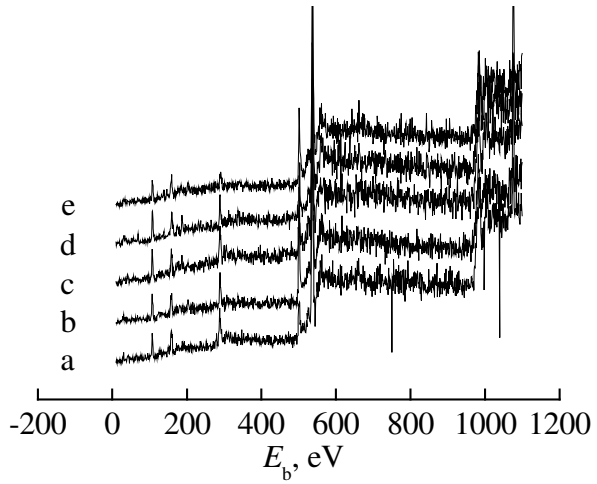

Fig. 2. XPS spectra of different catalysts (a) Xop-15 (b) Sop-16 (c) Fop-18 (d) Fop-21 (e) Fop-27

TABLE-3
CHARACTERISTIC PEAKS OF CRYSTALLINE PHASES IN MULTI-COMPONENT OXIDATIVE COUPLING OF METHANE CATALYSTS

Characteristic peaks	I	II	III
α-Cristobalite	21.8	36.0	31.3
Tridymite	21.6	20.5	23.3
SiO_2 (quartz)	26.7	20.8	50.2
Na_2SO_4	32.1	18.9	28.2
Na_2WO_4	32.5	16.8	27.5
Mn_2O_3	32.9	18.9	28.2
$Na_2Zr(PO_4)_2$	10.6	23.2	21.7

Comparing Tables 1 and 2, Sop-16 appears to have lower activity than the four other catalysts because no Mn_2O_3 or $Na_2Zr(PO_4)_2$ crystalline phases can be found in it. This indicates that Mn_2O_3[6,8,15] and zirconium compound[9,10] are the main components of catalyst activation, as reported in the literature.

X-Ray photoelectron spectroscopy: The representative XPS bands of Na 1s, S 2p, P 2p, Zr 3d and W 4f are shown in Figs. 2-4 and the corresponding binding energies and atomic ratios on the surface of the catalysts are summarized in Table-3. The binding energy of the Mn band was not found, possibly because the Mn content on the surface is less than 0.1 % and is too small to be detected by XPS. The binding energies of Na 1s, at 1072.21 and 1072.74 eV, indicate the presence of NaO_x. Additional energies of 1071.65, 1071.63 and 1071.19 eV show the state of Na_2SO_4. Two kinds of S species are clearly seen; the first has binding energies of S 2p at 163.82, 162.00 and 163.92 eV. This species is ascribed to the formation of a complex compound consisting of S and P, as evidenced by the

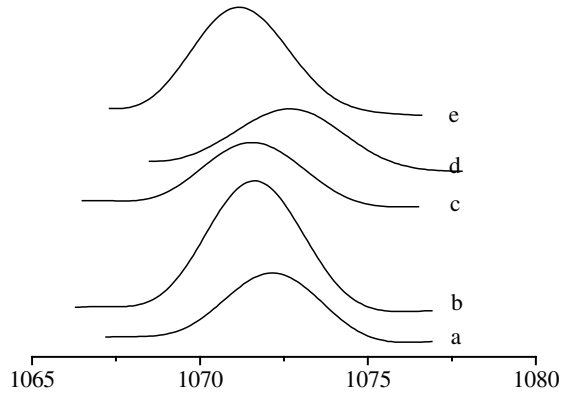

Na 1s

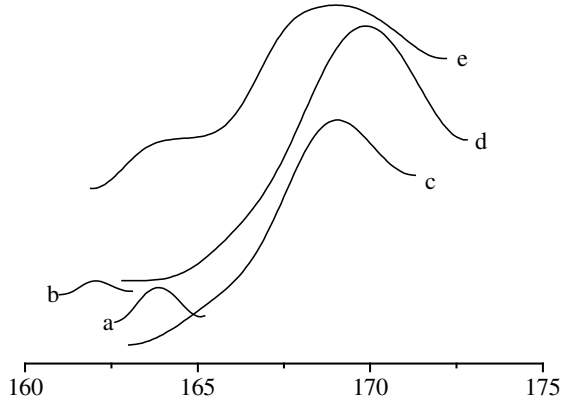

S 2p

TABLE-4
SURFACE ATOMIC RATIOS AND BINDING ENERGY OF VARIOUS ELEMENTS AT ROOM TEMPERATURE

Catalyst	Na (1s)		S (2p)		P (2p)		W ($4f_{7/2}$)		Zr ($3d_{5/2}$)	
	BE (eV)	at.	BE (eV)	at.	BE (eV)	at.	BE (eV)	at.	BE (eV)	at.
Xop-15	1072.21	1.0000	163.82	0.0268	133.50	0.0290	36.89	0.1117	–	–
Sop-16	1071.65	1.0000	162.00	0.0038	133.15	0.0130	35.76	0.1460	–	–
Fop-18	1071.63	1.0000	168.69	0.3266	131.73	0.0936	35.49	0.2180	182.80	0.0856
Fop-21	1072.74	1.0000	169.59	0.5005	–	–	–	–	183.13	0.2405
Fop-27	1071.19	1.0000	163.92	0.1856	132.48	0.0324	35.26	0.0827	182.42	0.0448

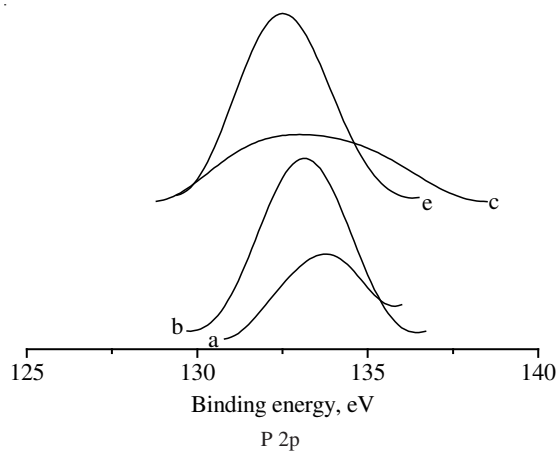

Fig. 3. High-resolution XPS Na 1s, S 2p, P 2p spectra (a) Xop-15 (b) Sop-16 (c) Fop-18 (d) Fop-21 (e) Fop-27

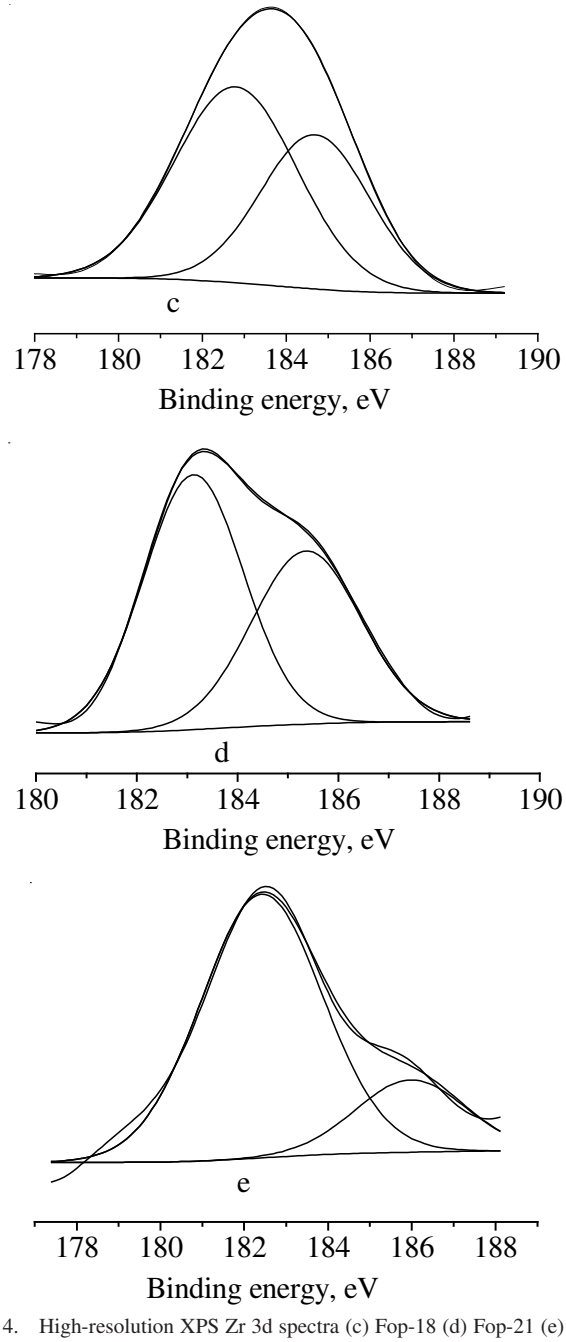

Fig. 4. High-resolution XPS Zr 3d spectra (c) Fop-18 (d) Fop-21 (e) Fop-27

binding energies of P 2p at 133.50, 133.15 and 134.61 eV. The second S species, with binding energies of 168.69 and 169.59 eV, indicate the presence of Na_2SO_4. A binding energy of 167.56 eV appears to indicate the presence Na_2SO_3. Zirconium binding energies of Zr 3d5/2, at 182.80, 183.13 and 182.42 eV, are believed to characterize a complex compound consisting of Zr, P, Cl and Na. W 4f7/2 binding energies of 35.76, 35.49 and 35.26 eV indicate the presence of a W-O species. However, the binding energy of W 4f7/2, at 36.89 eV, is diffcult to distinguish and is simply considered to indicate the presence of $WOCl_4$. Comparison of the XRD pattern and XPS spectra reveals that lack of Zr and Mn elements resulted in bad performance of Sop-16 catalyst. The presence and interaction of tridymite crystalline phase appear to cause the loss of Zr and Mn elements during the preparation. Surface atomic ratios and binding energies of the various elements in the catalysts are given in Table-4.

The O 1S XPS spectra are also studied (Fig. 5). The binding energy of O 1s in Xop-15 is 530.99 eV and is considered to indicate a lattice oxygen of Na_2WO_4, whereas the binding energy of O 1s, 531.75 eV, in Fop-21 appears to indicate a lattice oxygen of Na_2SO_4. There was also one peak for O 1s at 530.90 eV; this can be attributed to Na_2WO_4 or Na_2SO_4. Future studies may determine the accuracy of this supposition. Binding energy of O 1s, 535.95 eV, is not recognized in Sop-16.

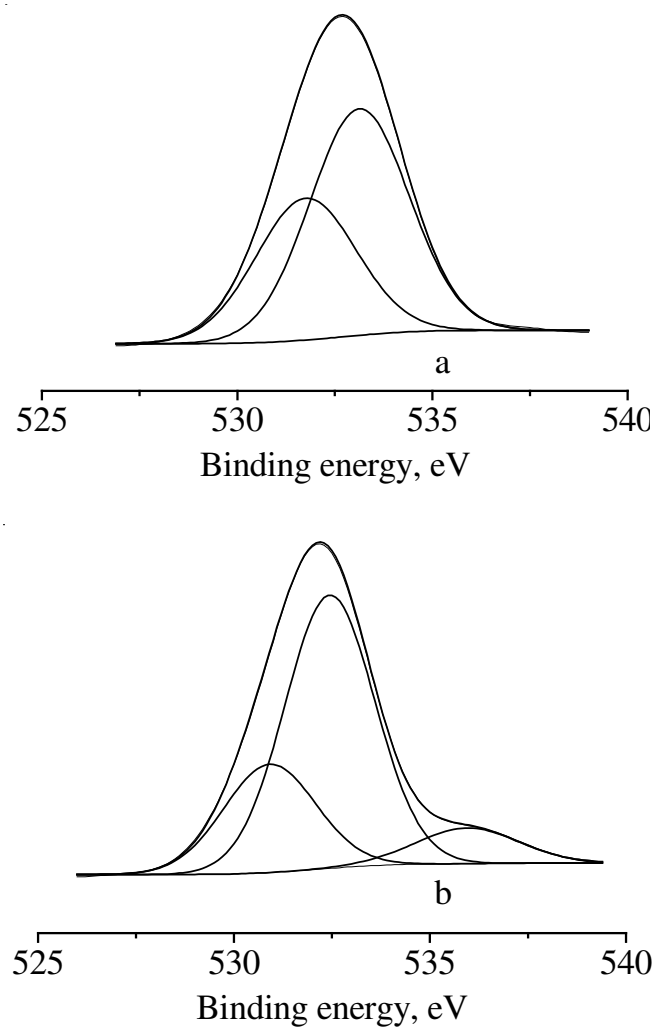

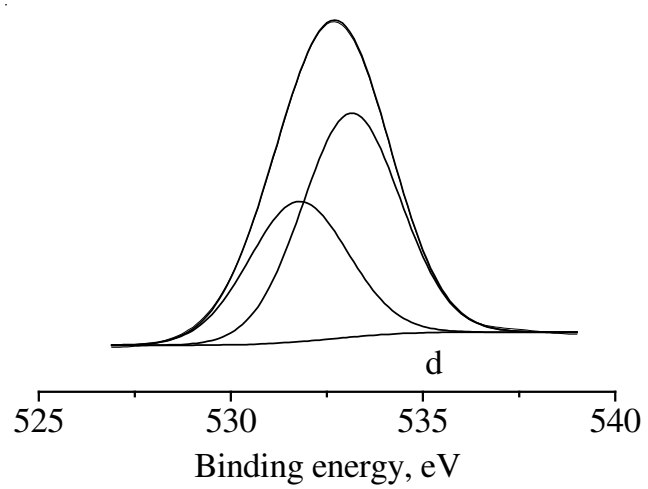

Fig. 5. High-resolution XPS O 1s spectra (a) Xop-15 (b) Sop-16 (d) Fop-21

FT-IR spectroscopy: Although the IR bands of the Mn_2O_3 and Zr components are not detected, the IR bands of α-cristobalite, amorphous SiO_2, quartz SiO_2 are distinguishable. The IR spectra of the five multi-component catalysts are shown in Fig. 6. The IR bands of the α-cristobalite are at 1100, 796, 620, 492 cm^{-1}. The IR band at 794 cm^{-1} reveals the presence of Na_2WO_4, which conforms to the illustration above. The IR bands of Xop-15, Fop-18, Fop-21 and Fop-27 are all similar to those from the Na-W-Mn-O/SiO_2 catalysts reported by Chua *et al.*[16], except for Sop-16 which had no IR band at 620 cm^{-1}. This deficient band indicates the difference between the α-cristobalite and tridymite phases. The tridymite phase is also cited for Sop-16's low activity. Comparing the IR bands of the catalysts with the Table-2, Table-1 reveal that the presence of Mn_2O_3 and $Na_2Zr(PO_4)$ have a close interaction with reactivity behaviours. The characteristic peaks of the five multi-component catalysts are summarized in Table-5.

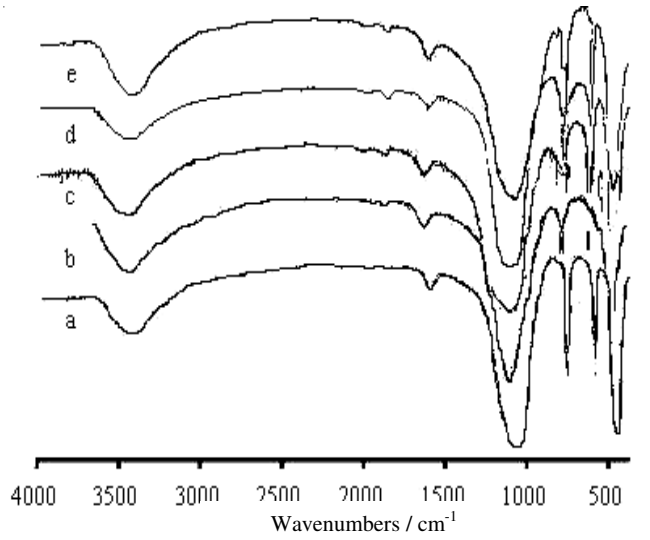

Fig. 6. FT-IR spectra of catalysts (a) Xop-15 (b) Sop-16 (c) Fop-18 (d) Fop-21 (e) Fop-27

Scanning electron microscopy: SEM micrographs obtained from Xop-15 and Fop-21 are shown in Fig. 7. From Fig. 7A, the crystal grains appear mainly on the surface of Xop-15. A pore channel can clearly be seen, but no floc can be found. Fig. 7B shows much floc and crystal grains co-exist on the SiO_2 carrier of Fop-21. This findings, along with Table-2 and previous research, indicate that the floc may be attributed to the complex compound consisting of Zr and P, while the crystal grains may be attributed to Mn_2O_3. Mn_2O_3 is considered to be the main active component of the catalysts and the addition of Zr efficiently improves their performance.

TABLE-5
CHARACTERISTIC PEAKS OF DIFFERENT CATALYSTS

Catalyst	Characteristic wavenumber (cm^{-1})
Xop-15	3447.00, 2017.82, 1893.65, 1636.65, 1097.81, 796.07, 620.26, 492.71
Sop-16	3447.23, 2017.86, 1893.65, 1636.35, 1104.52, 796.86, 490.13
Fop-18	3447.63, 2017.46, 1893.47, 1636.33, 1097.17, 796.00, 619.04, 492.74
Fop-21	3447.35, 2017.15, 1893.94, 1636.35, 1099.81, 795.53, 619.36, 489.72
Fop-27	3447.35, 2017.18, 1892.78, 1636.47, 1099.61, 794.58, 620.20, 491.31

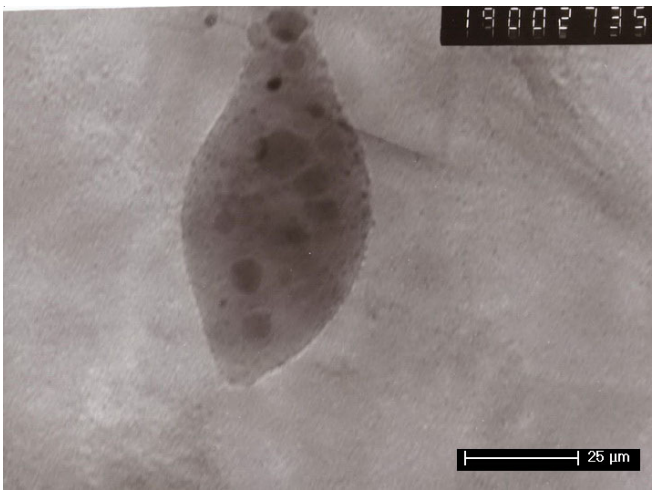

(A) Xop-15 (zoom in 2000 times)

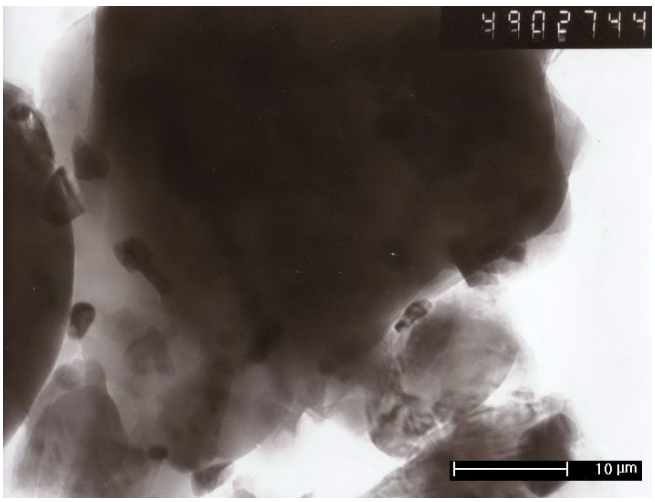

(B) Fop-21 (zoom in 5000 times

Fig. 7. SEM micrographs of the catalyst

Conclusion

Catalysts prepared from multiple components consisting of Na, Mn, Zr, W, S and P exhibited high activity and selectivity for oxidative coupling of methane. The highest methane conversion was 37.79 % with a C_{2+} selectivity of 73.50 % (C_{2+} yield 27.78 %). Analyses of the multi-component catalysts using XRD, XPS, FTIR and SEM provided the following useful information: the elements of the catalysts were mainly presented in the Mn_2O_3, Na_2SO_4, Na_2WO_4 and $Na_2Zr(PO_4)_2$ crystalline phases, Mn_2O_3 was considered to be the main active component of the catalysts and the addition of Zr efficiently improved the performance. It was suggested that the tridymite phase presented in the silica supports changed to the α-cristobalite phase after the addition of Na_2SO_4 and Na_2WO_4; α-cristobalite is the active carrier of the multi-component catalysts. The tridymite phase had no effect on the reaction performance. Sodium easily combined with WO_4; however, the role of WO_4 in the reaction remains unclear.

ACKNOWLEDGEMENTS

The authors are grateful to the financial supports from Department of Science and Technology of Jiangsu Province (BK2010198), Changzhou Municipal Science and Technology Bureau (CS20100004), State Key Laboratory of Green Chemical Synthesis Technology (GCTKF 2010013) and Natural Science Preliminary Research Foundation of Southeast University (XJ0619245).

REFERENCES

1. G.E. Keller and M.M. Bhasin, *J. Catal*., **73**, 9 (1982).
2. A. Malekzadeh, A. Khodadadi, A.K. Dalai and M. Abedini, *J. Natur. Gas Chem*., **16**, 121 (2007).
3. S. Kus, M. Otremba and M. Taniewski, *Fuel*, **82**, 1331 (2003).
4. K.M. Dooley, S.-Y. Chen and J.R.H. Ross, *J. Catal*., **145**, 402 (1994).
5. J.J. Tang, S.F. Ji, K. Wang and C.Y. Li, *Natur. Gas Chem. Ind*., **34**, 19 (2009).
6. S.-B. Li, *Chin. J. Chem.,* **19**, 16 (2001).
7. Z. Gholipour, A. Malekzadeh, R. Hatami, Y. Mortazavi and A. Khodadadi, J. Natur. Gas Chem., **19**, 35 (2010).
8. H.X. Wang, Research and Development of Catalyst on Methane Oxidative Coupling to C2 Hydrocarbons, Hangzhou: Zhejiang University (1998).
9. K.J. Yoon and H.L. Tung, *Appl. Catal. A: Gen*., **159**, 59 (1997).
10. K.J. Yoon and S.W. Seo, *Appl. Catal. A: Gen.*, **161**, L5 (1997).
11. K.J. Yoon and S.W. Seo, *Appl. Catal. B*, **7**, 237 (1996).
12. K. Huang, F.Q. Chen and D.W. Lu, *Appl. Catal. A: Gen*., **219**, 61 (2001).
13. K. Huang, X.L. Zhan, F.Q. Chen and D.W. Lv, *Chem. Eng. Sci*., **58**, 81 (2003).
14. W. Zheng, D.G. Cheng, N. Zhu, F.Q. Chen and X.L. Zhan, *J. Nat. Gas Chem*., **19**, 15 (2010).
15. S.-F. Ji, T.-C. Xiao, S.-B. Li, C.-Z. Xu, R.-L. Hou, K.S. Coleman and M.L.H. Green, *Appl. Catal. A: Gen*., **225**, 271 (2002).
16. Y.T. Chua, A.R. Mohamed and S. Bhatia, *Appl. Catal. A: Gen*., **343**, 142 (2008).